THE ASTROPHYSICAL JOURNAL, 237:596–612, 1980 April 15

ULTRAVIOLET, VISIBLE, INFRARED, AND X-RAY OBSERVATIONS OF SCORPIUS X-1

A. J. WILLIS AND R. WILSON
Department of Physics and Astronomy, University College London
P. VANDEN BOUT AND F. SANNER
Department of Astronomy, University of Texas at Austin
J. BLACK, R. J. DAVIS, A. K. DUPREE, H. GURSKY, L. HARTMANN, AND J. RAYMOND
Center for Astrophysics
T. MATILSKY
Physics Department, Rutgers University
M. BURGER[1,2]
Astronomical Institute, Space Research Laboratory, The Netherlands
C. DE LOORE[1]
Astrophysics Institute, Vrije Universiteit Brussel
E. L. VAN DESSEL[1]
Royal Belgium Observatory
P. WHITELOCK AND J. MENZIES
South African Astronomical Observatory
W. P. S. MEIKLE AND R. D. JOSEPH
Blackett Laboratory, Imperial College of Science and Technology, London
P. SANFORD AND G. POLLARD
Mullard Space Science Laboratory, England
AND
M. C. W. SANDFORD
SRC Appleton Laboratory, England
Received 1979 May 4; accepted 1979 October 16

ABSTRACT

The first ultraviolet spectroscopic observations of the X-ray source Scorpius X-1, obtained with the *IUE* satellite, together with complementary visible photometry and spectroscopy and infrared and X-ray photometry are presented and discussed. The UV data consist of low-resolution ($\Delta\lambda \approx 6$ Å) spectra covering the wavelength range $\lambda\lambda$1150–3200, with observations being recorded at many different phases and cycles in the $\sim 0^{d}.8$ binary period. The UV spectra show emission lines arising in Si II and IV; C III and IV; N III, IV, and V; O IV and V; and He II. No correlation is seen between the strengths of these lines with phase, but significant changes are observed when the source changes its UV and optical brightness. The optical H and He lines exhibit a similar behavior. The observed line-strength variations are probably the result of changing ionization conditions caused by a variable input X-ray flux in the line formation region.

Significant variations are observed in the UV continuum brightness of Sco X-1 which approximately match those observed simultaneously in the visible B band. The color excess of Sco X-1 is found to be $E_{B-V} = 0.35 \pm 0.05$ from the observed strength of the 2200 Å band. The UV continuum energy distribution of Sco X-1 has a steeper slope than predicted by models of the X-ray heated atmosphere of the primary star and is better fitted by a bremsstrahlung distribution.

Subject headings: infrared: sources — stars: individual — ultraviolet: spectra — X-rays: binaries

I. INTRODUCTION

Scorpius X-1 was the first nonsolar X-ray source discovered (Giacconi *et al.* 1962) and is the brightest X-ray source in the sky. It was also the first stellar X-ray source identified with a visible counterpart, the faint star V818 Sco (Sandage *et al.* 1966). The properties of the system and the nature of its optical, infrared, radio, and X-ray emission have recently been reviewed by Miyamoto and Matsuoka (1977). Although no X-ray eclipses are seen, the binary nature of the system has been confirmed both from visible photo-

[1] Material based on observations collected at the European Southern Observatory, La Silla, Chile.

[2] On leave from the Astrophysical Institute, Vrije Universiteit Brussel; holder of an ESA Fellowship.

metric measurements (Gottlieb, Wright, and Liller 1975) and spectroscopic observations (Cowley and Crampton 1975).

Sco X-1 was observed extensively with the *IUE* satellite during two observing runs (denoted hereafter as period I and period II) in 1978 April–May and July, assigned by the three *IUE* agencies (NASA, ESA, and SRC) for a coordinated program of observations of X-ray sources. The system was regarded as one of four "prime targets" involving full collaboration between the groups involved from the three agencies. The coordinated *IUE* observations of the other three "prime targets," Her X-1, Cyg X-1, and Vel X-1, will be reported in three other papers in the *Astrophysical Journal*. In addition, a program of observations of Sco X-1 at visible, infrared, and X-ray wavelengths was arranged for the *IUE* observing periods. The purpose of this paper is to present the *IUE* observations of Sco X-1 (the first ultraviolet spectroscopic observations of this source) and the complementary data obtained at the other observatories, together with a preliminary assessment and analysis of the acquired data.

II. ULTRAVIOLET OBSERVATIONS OF SCORPIUS X-1

a) Observations

The *IUE* satellite, its scientific instruments, and performance have recently been described by Boggess *et al.* (1978*a*, *b*). All the *IUE* observations of Sco X-1 reported here were obtained in the low-resolution spectroscopic mode ($\Delta\lambda \approx 6$ Å) and cover the full, available wavelength range of λλ1150–3200. Details of the *IUE* observations are given in Table 1, where the observation log has been arranged by spectrograph (SWP is the short-wavelength prime camera, λλ1150–2000; LWR is the long-wavelength redundant camera, λλ1900–3200) and for each spectrograph by increasing Julian Date number of the start of the exposures. Image SWP 1444 included data taken in both the small (3″ × 3″) and large (10″ × 20″) spectrograph entrance apertures; all other observations were recorded in the large aperture alone, where the full photometric integrity of the data is maintained.

Table 1 lists the camera image number, the JD of the start of the exposure, exposure time, and phase of the midpoint of the exposure. All Julian Dates quoted in this paper are heliocentric. The phases were calculated using the ephemerides of the Sco X-1 system given by Gottlieb, Wright, and Liller (1975), viz., period = $0^d.787313$, JD (zero phase) = 2,440,081.13, and all phases quoted throughout this paper have been determined using these values. The *IUE* observations that were obtained simultaneously with visible B-band photometry, visible spectroscopy, and infrared and X-ray photometry are so marked in Table 1.

The raw *IUE* data were reduced by the NASA and ESA observatories, as appropriate, at GSFC and Madrid, respectively, and include corrections for relative intensities, background, and wavelength scales.

The relative intensity data extracted from the *IUE* data tapes have been transformed to absolute energy fluxes (in ergs cm^{-2} s^{-1} $Å^{-1}$) using the *IUE* absolute energy calibration given by Bohlin *et al.* (1978). Prior to this calibration the effect of the strong geocoronal Lα line in the background data for the large-aperture images has been removed by interpolating in the background data uncontaminated by this line. A check has been made on the raw *IUE* images to ensure that no saturation effects exist in the data, and indeed no significant saturation was found in any of the *IUE* Sco X-1 images examined. A montage of representative SWP spectra of Sco X-1 is shown in Figure 1 and that for a selection of LWR images in Figure 2. These data and the spectral features observed are described in §§ II*b* and II*c*.

b) The Ultraviolet Energy Distribution of Scorpius X-1

In order to improve the accuracy of the data, the calibrated flux spectra have been smoothed over rectangular 50 Å passbands to give 17 broad-band flux measurements for the SWP spectra and 27 broad-band flux measurements for the LWR spectra. These data, denoted U_λ, are given in Table 2 for each image of Sco X-1.

In order to determine any phase dependence of the ultraviolet brightness of Sco X-1, we have compared the SWP data given in Table 2 with those for SWP 1470 (at phase ~0.0) and the LWR images with LWR 1434 (also at phase ~0.0). This has been done by forming the average ratio between the xth spectrum and the reference spectrum across the full *IUE* wavelength ranges according to the relations:

$$\Delta U(\mathrm{SWP}_x) = \left[\sum^{n} U_\lambda(\mathrm{SWP}_x)/U_\lambda(\mathrm{SWP\ 1470})\right]\Big/n$$

$$\Delta U(\mathrm{LWR}_x) = \left[\sum^{m} U_\lambda(\mathrm{LWR}_x)/U_\lambda(\mathrm{LWR\ 1434})\right]\Big/m$$

The resulting ratios in the mean UV flux for each image are plotted as a function of binary phase in Figure 3, together with the rms values for each image determined from the individual ΔU_λ for each spectrum.

As can be seen from Figure 3, the ΔU_λ data fall into two distinct groupings, representing high and low UV brightness levels ($\Delta U_\lambda > 0.7$ and $\Delta U_\lambda < 0.5$, respectively). A similar separation into high and low brightness levels is well known in the visible (Hiltner and Mook 1970). Similar gross changes in the visible brightness of Sco X-1 are observed to coincide with the UV brightness changes for those images with simultaneous B-band photometry (cf. § III*a*). Hereafter discussion of the *IUE* data will note whether the source was in a high or low UV brightness state with reference to Figure 3.

There is real evidence in Figure 3 for a significant variation in the UV brightness of the source in its high state, although the apparent light curve does not follow in detail the visible photometric-binary light curve determined by Gottlieb, Wright, and Liller (1975). These observed UV brightness variations are more likely similar to the flickering in intensity observed in the visible (cf. § III*a*).

A much lower level of variation is apparent in the low-state data shown in Figure 3. Observations in the visible also show a greatly reduced level of flickering

TABLE 1

IUE OBSERVATIONS OF SCORPIUS X-1

Image	JD start exp. 244 +	Exp. (min)	Phase	Notes
SWP 1444 *	3629.00	60.0	.3327	IR
SWP 1444	3629.05	20.0	.3786	IR
SWP 1452	3630.00	40.0	.5896	
SWP 1463	3631.22	35.0	.1354	
SWP 1467	3631.55	40.0	.5566	a,b
SWP 1468	3631.62	40.0	.6536	a,b
SWP 1470	3631.90	40.0	.0029	a,b
SWP 1490	3634.38	25.0	.1460	
SWP 1491	3634.46	30.0	.2514	
SWP 1953	3699.50	40.0	.8601	a,b,x
SWP 1954	3699.59	90.0	.9612	a,b,x
SWP 2033	3707.04	40.0	.4462	
SWP 2039	3707.74	40.0	.3344	
SWP 2040	3707.81	40.0	.4226	
SWP 2041	3707.87	40.0	.4926	
SWP 2048	3708.75	50.0	.6182	
SWP 2062	3710.71	50.0	.1121	
SWP 2063	3710.79	50.0	.2080	
SWP 2064	3710.85	50.0	.2822	
SWP 2065	3710.90	50.0	.3538	
SWP 2066	3710.97	50.0	.4366	
SWP 2076	3711.70	50.0	.3691	
SWP 2077	3711.78	50.0	.4609	
SWP 2078	3711.83	50.0	.5282	
SWP 2079	3711.88	50.0	.5940	
SWP 2080	3711.93	50.0	.6610	
LWR 1431	3631.59	40.0	.6068	a,b
LWR 1432	3631.66	40.0	.6950	a,b
LWR 1434	3631.94	40.0	.0505	a
LWR 1446	3634.43	40.0	.2109	
LWR 1804	3699.53	40.0	.9069	a,b,x
LWR 1846	3707.78	40.0	.3785	
LWR 1866	3710.76	40.0	.1623	
LWR 1872	3711.74	40.0	.4154	

* : image taken in the small spectrograph aperture.

a : simultaneous B-band photometry
b : simultaneous visible spectroscopy
x : simultaneous x-ray observations
IR : simultaneous IR observations

when the source is optically faint at $B \approx 13.3$. The light curve of the low-state ΔU shown in Figure 3 is similar to the visible photometric light curve determined by Gottlieb, Wright, and Liller (1975), although the amplitude of the UV curve ($\sim$0.1 mag) is less than that in the visible ($\sim$0.2 mag).

The low-state ΔU data shown in Figure 3 represent a mean decrease in brightness from the high-state data of $\sim$0.8 mag. A similar level of change was observed in the B-band monitoring of Sco X-1 for those observations performed simultaneously with *IUE* (cf. Fig. 10). This demonstrates that during these *large* brightness variations, the broad shape of the ultraviolet-B-band energy distribution has not altered significantly. Further discussion of this result will be given in §V.

The UV continuum energy distribution, formed by combining the U_λ broad-band fluxes for LWR 1434 and the continuum fluxes for SWP 1470 (shown in Fig. 1) with both observations recorded close to phase 0.9, is plotted on a magnitude scale in Figure 4.

The observed energy distribution is dominated by the strong interstellar 2200 Å feature. Nandy *et al.* (1975, 1976), from observations of many hundreds of reddened and unreddened early-type stars with the S2/68 ultraviolet sky-survey telescope, have determined the characteristics of the UV interstellar extinction curve in many different galactic regions. They conclude that the shape and level of the interstellar extinction curve is constant, within the small errors present in their data. Using the Nandy *et al.* (1975) extinction curve, the color excess of Sco X-1 can be determined

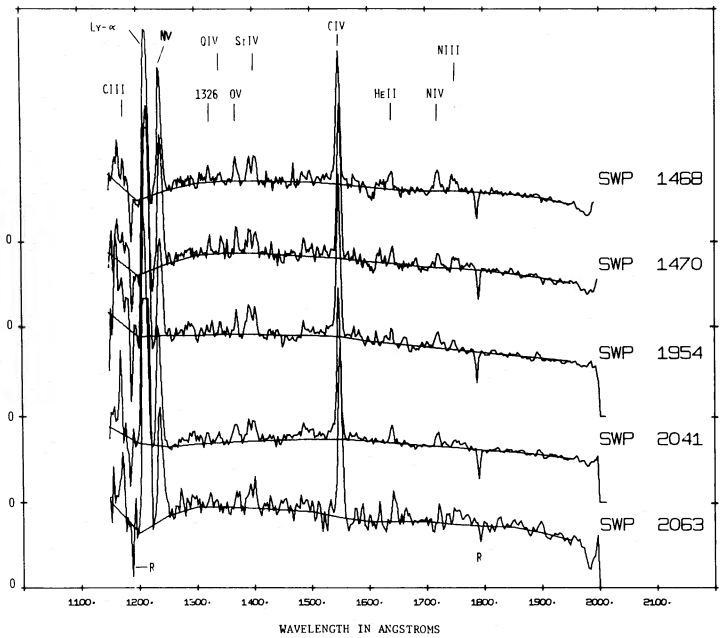

FIG. 1.—A montage of 5 SWP *IUE* spectra of Sco X-1. The individual spectra have been calibrated to absolute energy fluxes and are plotted on a linear intensity scale with the zero flux level marked in sequence with the spectra. The most prominent emission lines (discussed in the text) are marked. "R" shows the location of a camera reseau mark. The adopted continuum levels are plotted on each spectrum.

from the signature of its 2200 Å band, through a process of de-reddening the observed energy distribution until the 2200 Å band is removed. This process allows the color excess of the source to be determined accurately without recourse to any assumed intrinsic color for its energy distribution. The process of de-reddening is illustrated in Figure 4, showing the resulting energy distributions for Sco X-1 formed by de-reddening, using the color excesses labeling each curve, with each distribution normalized at λ2925. From Figure 4 we deduce that the color excess of Sco X-1 is 0.35 ± 0.05. This is somewhat higher than

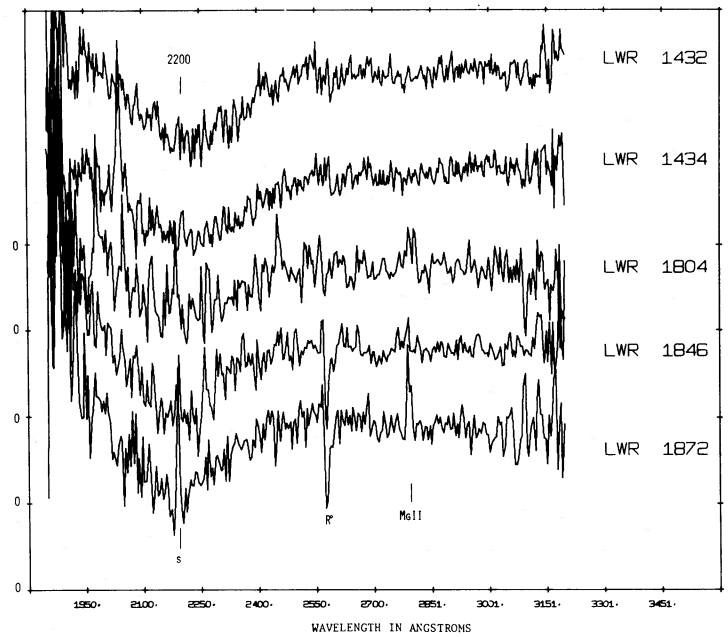

FIG. 2.—A montage of 5 LWR *IUE* spectra of Sco X-1. The individual spectra have been calibrated to absolute energy fluxes and are plotted on a linear-intensity ordinate scale with the zero flux level marked in sequence with the spectra. The most prominent spectral features, the interstellar 2200 Å band and the Sco X-1 Mg II λ2795, λ2802 resonance lines, are marked. "R" shows the location of camera reseaux and "S" that of a camera phosphor decay noise spike.

TABLE 2

IUE BROAD-BAND (50 Å) FLUXES (in units of 10^{-14} ergs cm^{-2} s^{-1} $Å^{-1}$)

Image	Phase	1175	1225	1275	1325	1375	1425	1475	1525	1575	1625	1675	1725	1775	1825	1875	1925	1975
SWP 1444	.333	17.9	42.3	17.5	18.0	19.1	19.2	18.0	19.8	21.6	16.2	14.5	16.1	14.2	13.8	13.4	11.3	10.4
SWP 1452	.590	24.1	40.1	21.6	22.9	24.6	23.8	24.0	24.3	28.2	20.3	18.6	19.6	18.6	17.3	17.2	14.7	12.6
SWP 1463	.135	16.1	81.6	18.5	20.9	20.9	19.7	18.5	21.4	21.7	16.7	15.7	17.0	14.9	15.2	14.2	12.9	10.5
SWP 1467	.557	20.3	37.5	24.7	25.8	28.3	25.5	25.6	30.1	26.2	22.3	21.6	22.6	20.4	20.6	19.0	16.5	13.5
SWP 1468	.654	20.9	34.6	20.6	22.3	23.3	22.3	21.8	26.3	23.4	19.5	17.7	19.6	17.1	17.0	16.1	14.1	11.5
SWP 1470	.003	24.6	38.4	24.9	27.1	28.5	26.5	25.9	29.2	28.9	23.1	21.3	21.9	20.3	19.5	18.1	15.9	13.9
SWP 1490	.146	19.8	51.6	20.7	25.2	24.1	23.7	22.8	26.8	27.2	19.4	19.0	19.1	16.6	19.5	16.7	16.1	11.0
SWP 1491	.251	24.9	39.8	23.8	24.4	25.3	21.3	23.3	27.1	25.4	23.4	20.7	19.0	15.1	18.5	16.1	15.9	11.8
SWP 1953	.860	7.7	25.6	12.2	12.6	12.6	12.8	12.1	13.5	12.0	10.4	9.9	10.6	9.7	9.8	9.3	6.9	6.7
SWP 1954	.961	14.4	25.7	11.8	11.8	12.6	11.7	11.2	14.0	12.4	10.6	9.8	10.2	8.7	8.6	8.3	7.6	6.9
SWP 2033	.446	28.3	62.3	17.5	17.5	18.7	18.2	19.2	21.4	21.2	16.8	15.6	16.1	14.9	14.8	14.3	12.8	11.5
SWP 2039	.334	18.0	39.1	18.6	19.3	20.9	20.0	21.0	25.6	22.0	19.1	17.0	18.2	15.8	16.0	15.6	14.4	11.7
SWP 2040	.423	18.5	38.5	17.8	17.5	20.1	18.7	19.2	20.6	22.6	17.2	15.8	16.8	14.9	14.4	14.5	12.6	12.1
SWP 2048	.618	20.3	35.8	16.4	17.0	18.1	17.5	18.1	19.4	23.1	17.3	15.1	15.1	14.4	13.5	12.6	11.7	10.6
SWP 2062	.112	11.5	28.6	12.5	12.6	13.2	12.2	12.9	14.5	14.5	11.5	10.1	11.2	10.0	9.6	9.5	8.3	6.7
SWP 2063	.208	11.2	29.8	11.5	11.6	12.1	11.6	11.4	12.4	11.7	9.8	9.6	9.5	9.3	8.7	8.4	7.1	5.3
SWP 2064	.282	12.1	31.8	11.6	11.5	12.5	12.3	12.6	13.7	13.3	10.5	9.4	10.1	9.2	9.2	9.2	7.9	6.6
SWP 2065	.354	11.7	34.0	12.0	12.1	13.3	12.2	13.2	14.7	14.0	10.8	10.0	10.9	9.4	9.5	9.4	8.4	7.2
SWP 2066	.437	10.7	39.1	11.6	12.0	13.0	12.1	12.7	15.2	14.2	11.1	10.8	10.9	9.7	9.5	9.4	8.0	6.6
SWP 2076	.369	11.3	27.6	12.3	11.9	12.6	12.2	12.8	13.2	14.0	11.3	10.6	11.4	10.2	9.8	9.6	8.5	6.3
SWP 2077	.461	14.0	29.7	12.3	12.3	13.5	12.7	13.0	14.5	15.0	12.1	10.9	11.1	10.0	10.1	9.8	8.7	6.3
SWP 2078	.528	14.2	32.1	12.3	11.9	13.0	12.7	13.2	14.8	15.1	12.0	11.1	11.6	10.5	9.9	9.8	9.3	7.1
SWP 2079	.594	12.8	33.3	12.7	12.6	13.4	13.1	13.5	14.6	15.1	11.9	11.0	11.4	10.4	10.1	10.0	9.0	6.5
SWP 2080	.661	11.4	34.2	11.9	11.6	12.5	12.4	13.1	14.1	14.8	11.4	10.3	10.8	10.2	9.8	9.6	8.5	6.6

Image	Phase	1875	1925	1975	2025	2075	2125	2175	2225	2275	2325	2375	2425	2475	2525
LWR 1431	.607	10.2	9.3	9.7	8.8	8.2	7.0	6.0	4.9	6.0	6.6	7.7	8.0	9.2	9.8
LWR 1432	.695	12.2	12.5	12.5	11.2	9.8	8.9	7.4	7.1	7.5	8.6	9.1	10.9	11.2	12.1
LWR 1434	.050	8.2	10.4	10.8	11.8	8.7	7.3	6.5	6.6	6.7	7.3	8.0	9.2	9.9	10.3
LWR 1446	.211	...	13.1	10.8	10.7	10.1	7.1	6.3	5.3	7.3	8.1	8.4	9.2	9.7	10.2
LWR 1804	.907	12.2	5.9	5.9	5.4	4.4	4.0	4.2	3.4	4.1	3.9	4.6	4.8	5.4	5.1
LWR 1846	.378	15.5	11.0	9.6	8.1	6.9	5.4	5.0	4.3	5.9	6.9	7.5	7.5	8.1	8.1
LWR 1866	.162	12.6	9.5	6.2	5.7	4.7	3.7	3.8	3.3	4.3	5.2	4.9	6.0	5.5	5.1
LWR 1872	.415	10.7	8.5	6.4	5.1	4.7	3.7	3.7	3.4	4.2	4.6	5.1	5.5	5.7	6.0

Image	Phase	2575	2625	2675	2725	2775	2825	2875	2925	2975	3025	3075	3125	3175
LWR 1431	.607	9.6	9.6	10.0	9.8	9.7	10.1	10.0	10.5	10.4	10.6	10.1	10.8	10.9
LWR 1432	.695	11.6	11.6	12.1	11.7	11.5	11.6	11.9	12.1	12.1	11.9	11.9	12.1	12.9
LWR 1434	.050	10.7	10.4	10.9	10.4	10.5	10.7	10.7	11.1	11.4	11.3	10.8	11.5	11.4
LWR 1446	.211	8.7	8.7	8.9	8.5	8.4	8.7	8.8	8.8	9.9	9.9	10.5	11.3	12.7
LWR 1804	.907	5.1	5.1	5.1	5.0	5.4	5.2	5.3	5.1	5.0	5.2	4.6	4.9	4.1
LWR 1846	.378	7.1	8.3	8.0	7.6	8.4	7.9	7.9	8.0	8.1	7.7	8.1	8.5	8.8
LWR 1866	.162	4.9	5.2	5.1	5.1	5.5	4.9	5.0	4.9	5.0	4.8	4.2	4.6	4.2
LWR 1872	.415	5.3	5.9	5.9	5.6	6.1	5.5	5.7	5.7	5.4	5.3	5.6	5.7	5.7

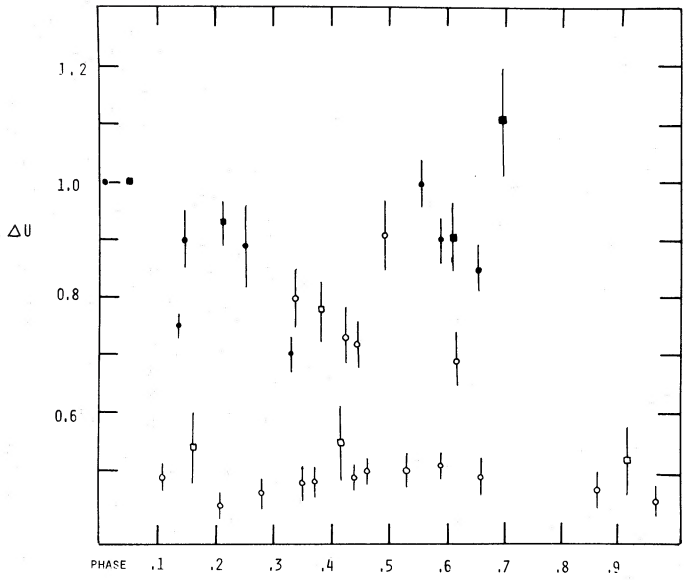

FIG. 3.—The brightness of the UV energy distribution of Sco X-1 relative to that at phase 0.0 (SWP 1470, LWR 1434), ΔU, plotted against binary phase. Filled circles are period I SWP spectra; open circles are period II SWP spectra; filled squares are period I LWR spectra, and open squares are period II LWR spectra.

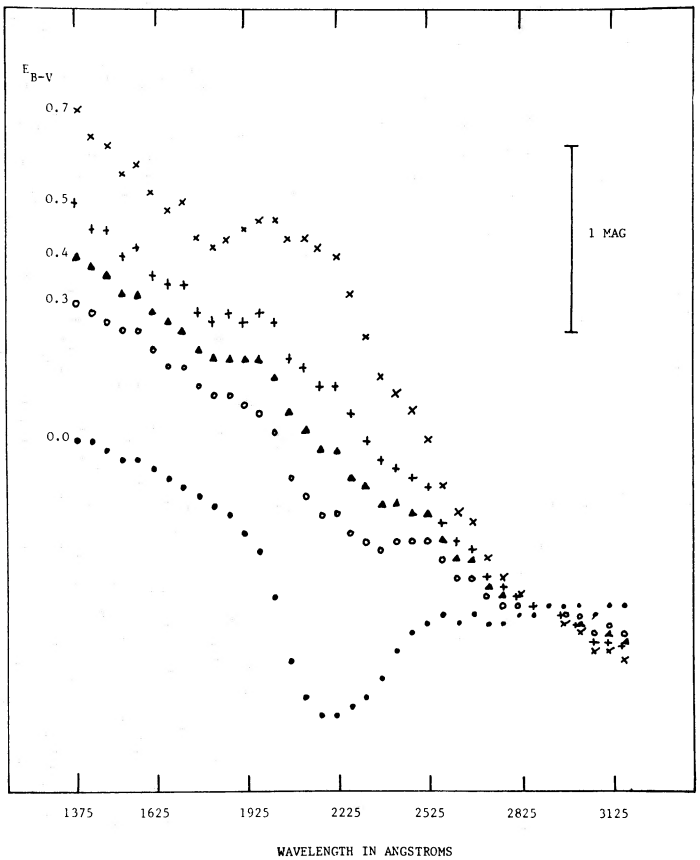

FIG. 4.—The observed UV energy distribution of Sco X-1 and the energy distributions corrected for interstellar reddening with several values of color excess E_{B-V}. The distributions are normalized at λ2795.

the value of 0.28 found by Wu (1979) on the basis of *ANS* ultraviolet photometry of Sco X-1. The small difference is probably due to the extinction curve used by Wu (1979), which differs from that determined by Nandy *et al.* (1975) in having a deeper 2200 Å feature and in the broad-band nature of the *ANS* photometry, which included no corrections for the effect of emission lines.

The loose nature of the correlation between color excess and distance in the direction of Sco X-1 (Sandage *et al.* 1966) at its high galactic latitude ($b^{II} \approx 24°$) makes a deduction of distance from the determined color excess uncertain. However, from the data of Sandage *et al.* (1966) and the determined color excess of $E_{B-V} = 0.35$, a distance to the source of more than 350 pc is implied.

c) *The Ultraviolet Spectrum of Scorpius X-1*

The short-wavelength UV spectra of Sco X-1 shown in Figure 1 are dominated by numerous, strong emission lines, the most prominent of which are marked in the figure and identified in Table 3. Only those features which appear on several of the SWP spectra have been regarded as real.

The absolute emission-line intensities of the most prominent of these emission lines and their equivalent widths have been determined by numerical integration over each line above an adopted continuum level, which has been drawn by eye on each spectrum, the eye estimate continua being shown as the full lines in Figure 1. The dip in the continua near λ1200 is consistent with the expected interstellar Lα scattering. The relative shapes of the continua, so drawn, for the SWP spectra are similar, providing a reasonable consistency check on the eye fits. The emission-line intensities and equivalent widths are given in Table 4, together with the mean values for each line, for the spectra obtained in the high and low UV brightness states of Sco X-1 highlighted in § II*b*, and the rms values for each line determined from the individual measurements. The errors in the line strengths and equivalent widths in the individual spectra are estimated as ~10% for C IV λ1550 and N V λ1240 and 20–30% for the other lines. The data in Table 4 demonstrate that there are no substantial variations (>25%) in the strengths of these UV emission lines during the periods when Sco X-1 was in either a high or low brightness state. The strengths of each line are plotted as a function of binary phase in Figure 5. No obvious variation in these data is coherent with orbital phase. The small variations that are apparent in the line strengths during the high-low brightness states are probably related to the small-scale flickering in the X-ray emission from the source which is known to occur (White *et al.* 1976), resulting in a fluctuation in the ionization energy supplied by the X-ray source.

TABLE 3

EMISSION LINES OBSERVED IN THE SWP ULTRAVIOLET SPECTRUM OF SCORPIUS X-1

Feature	Transition	Comments
C III 1175.....	$2p\ ^3P^o$–$2p^2\ ^3P$	low-sensitivity part of *IUE* SWP image
H I 1215.....	$1s\ ^2S$–$2p\ ^2P^o$	mainly geocoronal
N V 1240.....	$2S\ ^2S$–$2p\ ^2P^o$	
λ 1326.....	...	possible
O IV 1343.....	$2p^2\ ^2P^o$–$2p^3\ ^2D^o$	
O V 1370.....	$2p\ ^1P^o$–$2p^2\ ^1D$	
Si IV 1393.....	$3s\ ^2S$–$3p\ ^2P^o$	
Si IV 1402.....	$3s\ ^2S$–$3p\ ^2P^o$	
N IV 1490.....	$2s\ ^1S$–$2p\ ^3P^o$	
Si II 1525.....	$3p\ ^2P^o$–$4s\ ^2S$	possible
C IV 1550.....	$2s\ ^2S$–$2p\ ^2P^o$	
He II 1640.....	$2p\ ^2P^o$–$3d\ ^2D$	
N IV 1718.....	$2p\ ^1P^o$–$2p^2\ ^1D$	
N III 1750.....	$2p\ ^2P^o$–$2p^2\ ^4P$	

The emission-line intensities in the high and low brightness states are, however, significantly different. The ratio of the high/low line intensities is given for each line in Table 4. There is a clear indication that this ratio is greater for the higher ionization lines in O V and N V than in C IV, He II, and N IV. The spectra SWP 1953 and SWP 1954 were obtained when Sco X-1 was observed in a low X-ray brightness state (cf. § IV). Again this indicates that the source of the variable emission-line strengths is the varying, ionizing X-ray flux from the compact object in the Sco X-1 system. Similar, ionization-linked variations are observed in the strengths of the visible hydrogen and helium lines between high and low X-ray emission levels (cf. § III*b*).

The most prominent feature in the long-wavelength spectra of Sco X-1 (Fig. 2) is the strong, broad interstellar 2200 Å band discussed above. In the period II spectra, taken when the source was in a low brightness state, the Mg II λ2795, λ2802 resonance doublet appears strongly in emission, again in line with the expected varying ionization conditions in the emission-line formation region of the system.

III. VISIBLE AND INFRARED OBSERVATIONS OF SCORPIUS X-1

a) *B-Band Photometry*

Sco X-1 is known to exhibit irregular visible light variations, with time scales ranging from seconds to days (Mook *et al.* 1975). In order to ensure good time resolution in the ground-based photometry complementing the *IUE* observations, the visible photometric monitoring was restricted to the Johnson B band alone. Observations of Sco X-1 were made on May 2–3 in period I and July 8–9 and July 9–10 in period II, using the 1.0 m telescopes at the South African Astronomical Observatory (SAAO) at Sutherland and at ESO on La Silla, Chile. Although the period of the optical monitoring was rather restricted, data were obtained simultaneously with several of the *IUE* observations as desired, providing the first, simultaneous, visible and vacuum UV observations of Sco X-1. Both telescopes were equipped with pulse-counting photoelectric cooled EMI 6256 photomultipliers.

Integration times of 10 s were used for the *B*-filter observations, and the comparison star BD −15°4301 was monitored at both observatories at intervals of ~15 minutes. The data were corrected for extinction with the zero point determined by comparison with BD −15°4301 alone, a full transformation to the

TABLE 4

A. Ultraviolet Emission-Line Intensities and Equivalent Widths

Image	Phase	N v λ1240	O v λ1370	Si iv λ1400	C iv λ1550	He ii λ1640	N iv λ1718
SWP 1444(H).....	.333 I_λ	4.1 (−12)	3.5 (−13)	1.3 (−12)	4.0 (−12)	4.3 (−13)	4.7 (−13)
	W_λ	28.2	2.1	7.6	24.3	2.8	3.1
SWP 1452(H).....	.590 I_λ	4.6 (−12)	5.6 (−13)	1.1 (−12)	4.5 (−12)	5.9 (−13)	6.2 (−13)
	W_λ	25.8	2.5	5.0	22.0	3.1	3.4
SWP 1463(H).....	.135 I_λ	4.3 (−12)	6.2 (−13)	1.4 (−12)	4.1 (−12)	5.0 (−13)	5.6 (−13)
	W_λ	28.8	3.4	7.6	24.6	3.1	3.6
SWP 1467(H).....	.556 I_λ	4.5 (−12)	8.9 (−13)	1.3 (−12)	3.7 (−12)	3.1 (−13)	4.4 (−13)
	W_λ	21.0	3.6	5.2	15.8	1.4	2.1
SWP 1468(H).....	.654 I_λ	3.9 (−12)	5.1 (−13)	1.2 (−12)	3.7 (−12)	6.7 (−13)	7.5 (−13)
	W_λ	22.9	2.4	5.6	18.6	3.7	4.3
SWP 1470(H).....	.003 I_λ	4.4 (−12)	6.0 (−13)	1.2 (−12)	4.1 (−12)	3.8 (−13)	5.0 (−13)
	W_λ	20.7	2.3	4.8	17.3	1.7	2.4
SWP 1953(L).....	.860 I_λ	1.5 (−12)	8.7 (−14)	5.7 (−13)	2.1 (−12)	3.7 (−13)	3.6 (−13)
	W_λ	15.1	0.7	4.7	20.0	3.8	3.8
SWP 1954(L).....	.961 I_λ	1.3 (−12)	1.6 (−13)	6.1 (−13)	1.8 (−12)	1.6 (−13)	2.7 (−13)
	W_λ	11.2	1.4	5.4	16.4	1.6	2.8
SWP 2033(H).....	.446 I_λ	2.3 (−12)	5.2 (−13)	1.1 (−12)	3.3 (−12)	4.4 (−13)	4.1 (−13)
	W_λ	13.4	3.2	6.7	19.8	2.9	2.8
SWP 2039(H).....	.334 I_λ	3.5 (−12)	4.8 (−13)	7.4 (−13)	3.7 (−12)	5.3 (−13)	6.4 (−13)
	W_λ	21.9	2.6	3.9	19.8	3.0	3.8
SWP 2040(H).....	.423 I_λ	3.2 (−12)	6.9 (−13)	1.4 (−12)	3.6 (−12)	2.8 (−13)	5.5 (−13)
	W_λ	21.3	4.1	8.1	21.4	1.7	2.9
SWP 2041(H).....	.493 I_λ	4.0 (−12)	6.0 (−13)	1.2 (−12)	4.1 (−12)	4.8 (−13)	5.7 (−13)
	W_λ	20.5	2.8	5.7	18.8	2.3	2.9
SWP 2048(H).....	.618 I_λ	2.9 (−12)	4.0 (−13)	9.0 (−13)	3.7 (−12)	4.6 (−13)	2.1 (−13)
	W_λ	19.4	2.4	5.5	21.0	2.9	1.4
SWP 2062(L).....	.112 I_λ	1.9 (−12)	2.4 (−13)	7.2 (−13)	2.6 (−12)	3.9 (−13)	5.4 (−13)
	W_λ	17.9	2.0	6.2	23.7	3.8	5.5
SWP 2063(L).....	.208 I_λ	1.6 (−12)	2.0 (−13)	5.0 (−13)	2.1 (−12)	3.2 (−13)	1.6 (−13)
	W_λ	17.4	1.8	4.6	21.3	3.4	1.8
SWP 2064(L).....	.282 I_λ	1.7 (−12)	1.4 (−13)	5.8 (−13)	2.6 (−12)	2.5 (−13)	1.6 (−13)
	W_λ	17.6	1.2	4.9	24.0	2.5	1.7
SWP 2065(L).....	.354 I_λ	1.5 (−12)	2.6 (−13)	5.7 (−13)	2.0 (−12)	2.7 (−13)	3.9 (−13)
	W_λ	14.9	2.1	4.7	17.0	2.7	3.9
SWP 2066(L).....	.437 I_λ	1.8 (−12)	1.3 (−12)	3.0 (−13)	2.5 (−12)	2.5 (−13)	2.4 (−13)
	W_λ	19.2	1.1	2.5	21.7	2.3	2.4
SWP 2076(L).....	.369 I_λ	1.6 (−12)	2.2 (−13)	4.5 (−13)	2.1 (−12)	3.0 (−13)	3.9 (−13)
	W_λ	16.1	1.9	3.9	18.8	2.8	3.7
SWP 2077(L).....	.461 I_λ	1.7 (−12)	2.3 (−13)	7.7 (−13)	2.5 (−12)	3.6 (−13)	3.5 (−13)
	W_λ	15.5	1.9	6.4	21.0	3.3	3.4
SWP 2078(L).....	.528 I_λ	2.0 (−12)	1.6 (−13)	7.5 (−13)	2.5 (−12)	3.7 (−13)	2.8 (−13)
	W_λ	19.7	1.3	6.3	20.6	3.3	2.7
SWP 2079(L).....	.594 I_λ	1.7 (−12)	1.4 (−13)	5.8 (−13)	2.3 (−12)	1.8 (−13)	2.8 (−13)
	W_λ	17.1	1.2	4.7	19.6	1.6	2.7
SWP 2080(L).....	.661 I_λ	1.8 (−12)	1.4 (−13)	3.8 (−13)	2.5 (−12)	4.3 (−13)	3.2 (−13)
	W_λ	17.0	1.2	3.2	21.7	4.2	3.2

B. Average Line Intensities for the High (H) and Low (L) Brightness State Spectra and Ratio Between Line Intensities for High/Low Brightness States

Line	H Spectra	L Spectra	H/L
N v λ1240:			
$\bar{I}_\lambda$.....	3.8 ± .7 (−12)	1.7 ± .2 (−12)	2.26
$\bar{W}_\lambda$.....	22.2 ± 4.3	16.6 ± 2.3	1.34
O v λ1370:			
$\bar{I}_\lambda$.....	5.6 ± 1.4 (−13)	1.7 ± .5 (−13)	3.21
$\bar{W}_\lambda$.....	2.8 ± .6	1.5 ± .4	1.92
Si iv λ1400:			
$\bar{I}_\lambda$.....	1.2 ± .2 (−12)	5.6 ± 1.4 (−13)	2.07
$\bar{W}_\lambda$.....	6.0 ± 1.3	4.8 ± 1.2	1.24
C iv λ1550:			
$\bar{I}_\lambda$.....	3.9 ± .3 (−12)	2.3 ± .3 (−12)	1.68
$\bar{W}_\lambda$.....	20.3 ± 2.7	20.5 ± 2.3	0.99
He ii λ1640:			
$\bar{I}_\lambda$.....	4.6 ± 1.1 (−13)	3.0 ± .8 (−13)	1.51
$\bar{W}_\lambda$.....	2.6 ± .7	2.9 ± .8	0.88
N iv λ1718:			
$\bar{I}_\lambda$.....	5.2 ± 1.4 (−13)	3.1 ± 1.1 (−13)	1.66
$\bar{W}_\lambda$.....	3.0 ± .8	3.1 ± 1.0	0.97

Note.—Line intensities, I_λ, are in ergs cm^{-2} s^{-1}; equivalent widths, W_λ, are in Å. High brightness state spectra are marked "H"; low brightness spectra are marked "L."

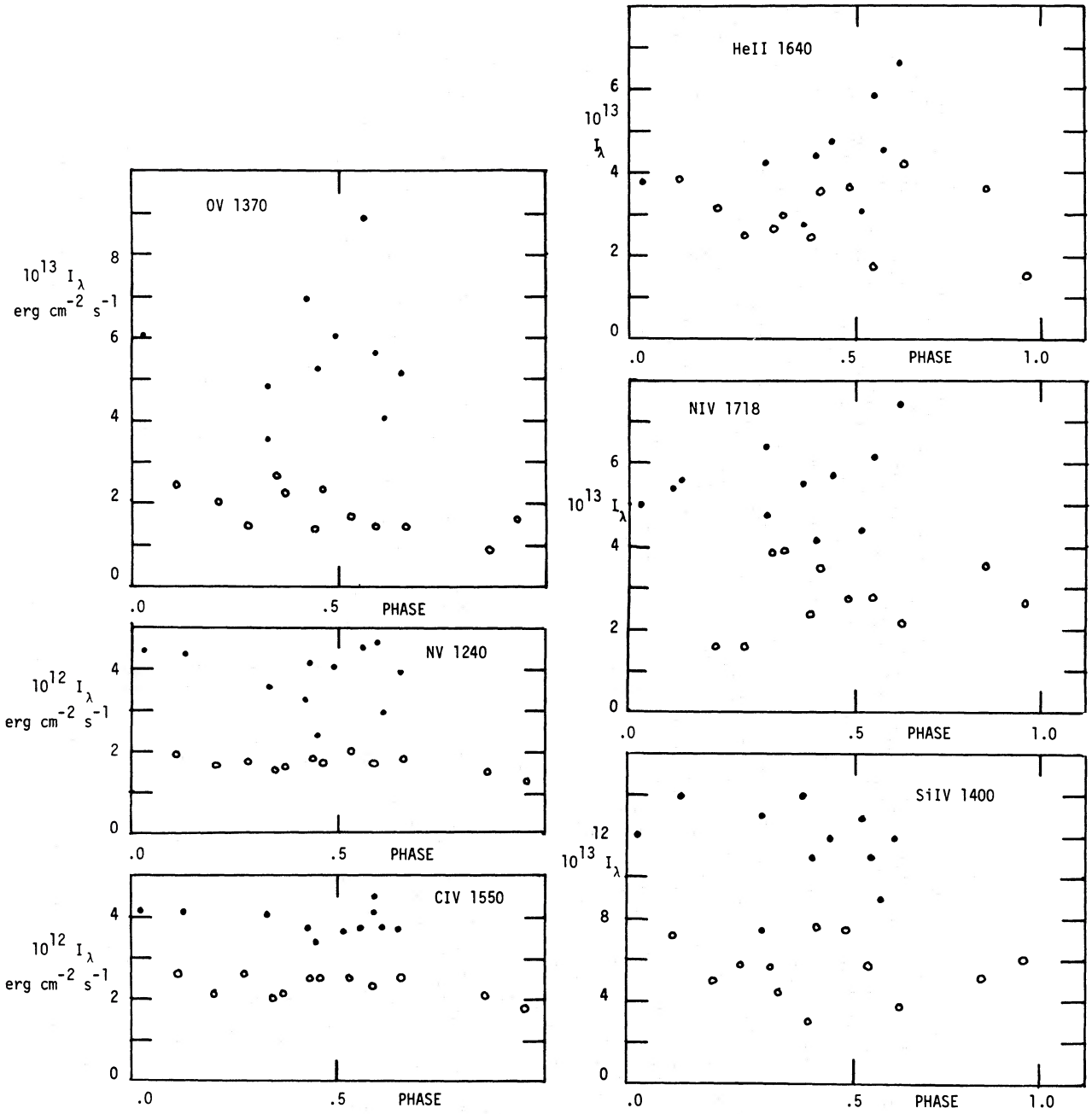

FIG. 5.—The N v λ1240, O v λ1370, Si iv λ1400, C iv λ1550, He ii λ1640, and N iv λ1718 emission-line intensities observed in the SWP spectra of Sco X-1, plotted as a function of binary phase. Filled circles are line strengths measured in the high UV brightness state spectra; open circles are measurements in the low UV brightness state spectra (see text).

standard system being impossible without $(B - V)$ measurements. The standard deviation on the measurements of the comparison star was 0.004 mag for all the observing nights, confirming the nonvariability of this star (Ilovaisky 1978). This value of 0.004 mag is taken as an upper limit to the errors introduced by uncertainties in extinction corrections. Figures 6*a* and 6*b* show the determined *B*-magnitudes of Sco X-1, as a function of Julian Date of observation for the period I and period II observations, respectively. The errors in these data have been assessed using photon statistics on the observed count rates for Sco X-1 and include the sky correction uncertainty given above. The errors are determined as 0.007 mag for May 2–3 and July 8–9 and 0.010 mag for July 9–10.

On the night of May 2–3 (Fig. 6*a*) Sco X-1 exhibited considerable intrinsic variability in its *B*-magnitude. Short time-scale flickering is evident with occasional large (~0.96 mag) outbursts. During the period II monitoring (Fig. 6*b*) the short time-scale flickering is

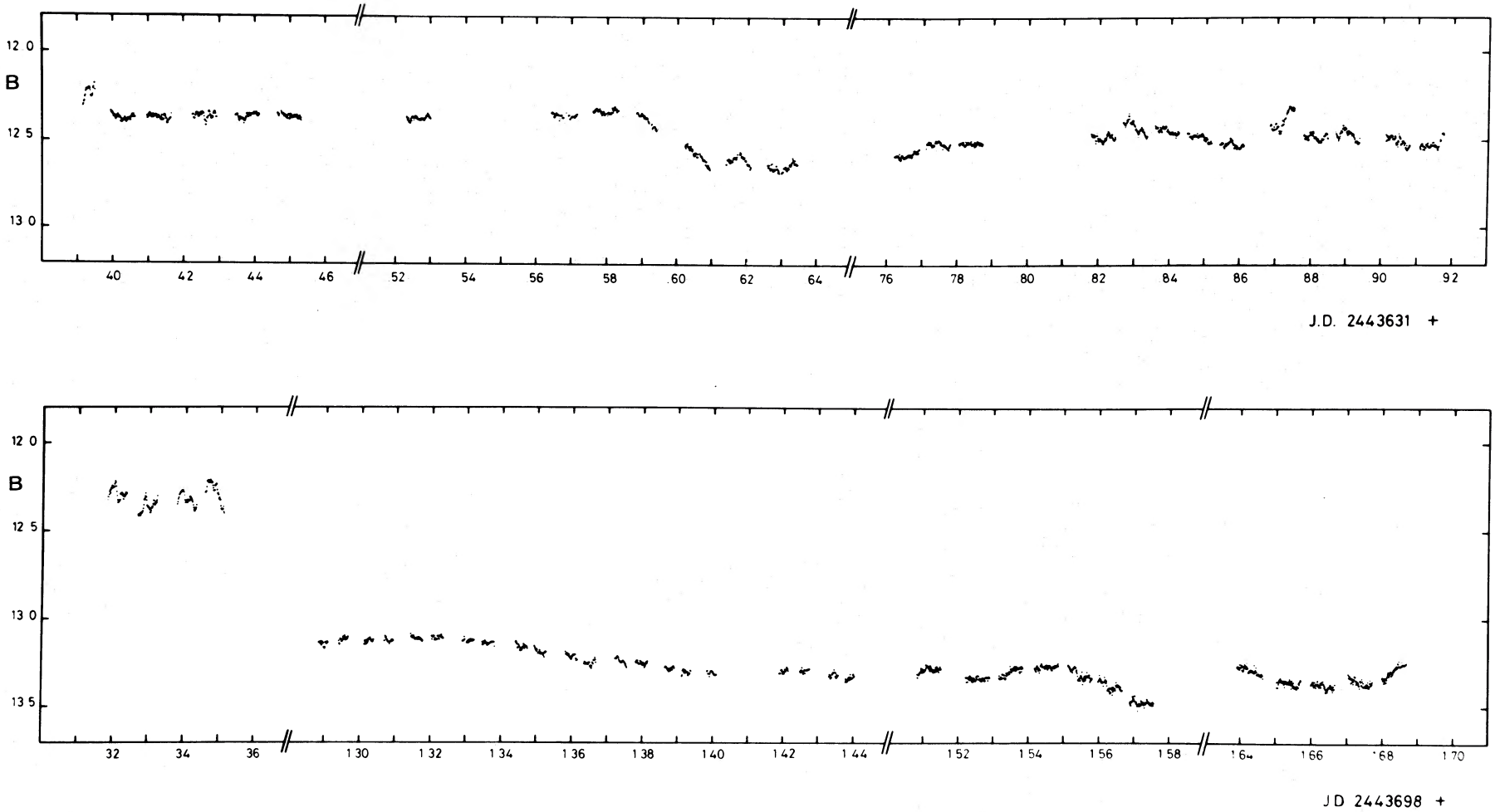

FIG. 6.—*B*-magnitude of Sco X-1 versus Julian Date for (*top*) the period I observations, with the data between JD fraction .38 and .64 being obtained at SAAO and those between .75 and .90 at ESO, and (*bottom*) the period II observations, with those between JD fraction .31 and 1.45 being obtained at SAAO and those between 1.50 and 1.69 at ESO. The small regular gaps in the data are due to the time required to observe the comparison star. The large gaps are due to unreliable weather conditions. The errors in these data lie between 0.007 mag and 0.010 mag (see text).

evident in the observations of July 8–9 when the source was in a bright state, but considerably less activity is present on July 9–10 when the source had decreased in brightness to ~13.2 mag. The most extreme change in these latter data is ~0.06 mag in 5 minutes.

The *B*-magnitude variations shown in Figure 6 and discussed above show no coherence with the visible photometric light curve for the system given by Gottlieb, Wright, and Liller (1975), probably mainly as a result of the flickering of the source which is superposed on any binary light curve. The behavior of Sco X-1 during the two *IUE* observing periods is similar to previously reported visible photometric observations. In general Sco X-1 shows activity in both the optical and X-ray wavelength ranges when $m_B \leq 12.7$ and is quiescent at fainter brightness levels (Mook *et al.* 1975).

b) Visible Spectroscopy

Ground-based, visible spectroscopic monitoring of Sco X-1 was obtained during period I and period II at both La Silla and SAAO. A log of the SAAO spectroscopic observations is given in Table 5. These spectra were recorded using the Cassegrain image-tube spectrograph of the 1.9 m telescope and cover the wavelength ranges λλ4100–4900 for the IIa-O blue plates and λλ4300–5700 for the 3AJ red plates at reciprocal dispersions of 30 Å mm^{-1} and 75 Å mm^{-1}, respectively. A log of the La Silla spectroscopic observations is given in Table 6. These spectra were obtained with the ESO 1.52 m telescope and echelle spectrograph (Echelec), and each spectrum covers the wavelength range λλ3600–5600 at a reciprocal dispersion of about 124 Å mm^{-1} (except for plate P1135

TABLE 5

LOG OF THE SAAO SPECTROSCOPY OF SCORPIUS X-1 AND THE MEASURED EQUIVALENT WIDTHS OF THE EMISSION LINES: He II λ4686, Hβ, Hγ, AND N III/C III λ4640

PLATE	JD (mid-exp.) (2,440,000+)	EMULSION	EXP. (min)	EQUIVALENT WIDTHS (Å) He II λ4686	Hβ	Hγ	N III/C III λ4640
CX 1804a	3631.40208	IIa-O	6				
b	.40799		5				
c	.41493		5	2.75	1.09	0.59	2.96
e	.42535		5				
f	.43021		5				
CX 1805a	3631.43924	IIa-O	5				
b	.44410		5				
c	.45035		5				
d	.45556		6	2.24	1.71	0.81	3.16
e	.46111		6				
f	.46632		5				
CX 1806a	3631.51632	IIa-O	3				
b	.52014		5				
c	.52465		5				
d	.52847		3	2.25	0.95	0.19	4.11
e	.53160		3				
f	.53452		5				
CX 1807a	3631.56597	IIa-O	4				
b	.56944		4				
c	.57361		4				
d	.57703		4	1.52	0.39	0.11	2.54
e	.58090		4				
f	.58472		4				
CX 1808a	3631.59444	IIa-O	4				
b	.59792		4				
c	.60208		4				
d	.60704		6	2.23	1.50	0.22	3.11
e	.61250		5				
f	.61701		5				
CX 1991a	3699.29792	IIIa-J	40	1.54	6.48	1.67	3.18
b	.32396		27	1.39	6.63	1.24	2.61
CX 1992a	3699.36562	IIIa-J	35	1.26	6.59	1.61	2.67
b	.39306		40	1.17	5.57	1.75	3.02
c	.42292		40	1.22	5.72	1.68	3.02
d	.45694		50	1.37	4.97	1.72	2.46
CX 1996a	3700.29826	IIIa-J	15	...	...	...	...
b	.31007		15	...	...	...	...
CX 1998a	3700.43819	IIIa-J	30	1.48	1.68	0.20	3.54
b	.46354		35	1.74	0.80	0.23	3.96

NOTE.—The average values of the equivalent widths of each line are given for the individual spectra of plates CX 1804–1808.

TABLE 6

LOG OF THE ESO VISIBLE SPECTROSCOPY OF SCORPIUS X-1

Plate	JD (2,440,000+)	Exp. (min)	Phase	Radial Velocity (He II λ4686; km s^{-1})
P119.....	3630.743	30	0.556	−163
P1120A.....	3630.793	30	0.618	−120
P1120B.....	3630.822	35	0.655	−124
P1121A.....	3630.853	45	0.695	−101
P1121B.....	3630.881	35	0.731	−92
P1122.....	3630.910	40	0.768	−139
P1133.....	3631.774	80	0.865	(−153)[b]
P1134.....	3631.839	30	0.948	−52
P1135[a].....	3631.866	40	0.981	
P1136.....	3631.896	40	0.019	−45
P1137.....	3631.922	30	0.053	−54
P1156.....	3699.638	30	0.053	−99
P1157.....	3699.661	30	0.082	
P1158.....	3699.690	30	0.118	−82
P1159.....	3699.714	35	0.148	−87

[a] Reciprocal dispersion 62 Å mm^{-1}.

[b] Asymmetric line.

taken at 62 Å mm^{-1}, although in general the violet part of each spectrum is poorly exposed.

The characteristics of the visible spectrum of Sco X-1 have been described by Cowley and Crampton (1975) and by Crampton *et al.* (1976). The basic nature of the spectrum described in these two papers is similar to that observed in the La Silla and SAAO spectra described herein. As a result of the short exposures employed, particularly for the SAAO spectra with multiple exposures being recorded on each plate, it is possible to observe short time-scale changes in the strengths of several emission lines. Rapid changes are observed in the strengths and profiles of the Hγ, Hβ, λλ4630–4660 complex, and He II λ4686 emission lines in the spectra taken on SAAO plates CX 1804 and CK 1805. In these data the He II 4686 line is seen to be double peaked with a separation corresponding to 200 km s^{-1}. Asymmetries in the λ4686 emission line seem to occur in the spectra of plate P1133 and (less so) in plate P1134. These could be related to the flickering that was noted photometrically at that time. Also seen in the spectra on plates CX 1804 and CX 1805 is a strong absorption feature at λ4620, which is variable in strength and is quite sharp in the spectra on plate CX 1804, but considerably broader on plate CX 1805. The N v λ4603, λ4619 lines reported by Crampton *et al.* (1976) are seen in these spectra and are found to vary in strength on time scales of ~5 minutes. Although the He II λ4686 line exhibits a complex pattern of components, the peak emission of the strongest component is well defined, and included in Table 6 for the La Silla spectra are the radial velocities of this strong component in the He II λ4686 line measured during the wavelength calibration of the data. These radial velocities are in excellent agreement with those derived from the spectroscopic velocity curve for the system determined by Cowley and Crampton (1975), confirming their determined spectroscopic period for the system of 0^{d}.7873.

A montage of the visible spectra of Sco X-1, covering the wavelength ranges encompassing the lines Hγ, λλ4620–4660, He II λ4686, and Hβ from the SAAO spectra is shown in Figure 7, and that for the same wavelength regions in the La Silla spectra is shown in Figure 8. The emission features are seen to exhibit a complex structure, implying the presence of several streams of material moving with different velocities in the Sco X-1 system. Equivalent widths of the Hγ, Hβ, He II λ4686, and N III/C III λλ4640 complex observed in the SAAO spectra are given in Table 5.

Both the SAAO and La Silla spectra show that, during the period I, *IUE* observations the λλ4620–4660 emission complex and He II λ4686 are considerably stronger in emission than both Hγ and Hβ; indeed in some spectra taken during these times the hydrogen lines appear to be absent. In period II, when Sco X-1 is in a low optical (and ultraviolet) brightness state (CX 1991, 1992, P1156–9), the λλ4620–4660 complex and He II λ4686 are considerably weaker, while there is a great increase in emission strength of the hydrogen lines. These changes in the hydrogen and helium lines with the visible brightness of Sco X-1 are similar to those previously reported by Mook, Hiltner, and Lynds (1971) and Mook, Edwards, and Hiltner (1972). These changes are consistent with the observed variations of the UV lines described in § II*c*, interpreted in terms of varying, X-ray ionizing energy from the source, when Sco X-1 is optically bright and faint.

c) Infrared Observations

Sco X-1 was observed with our near-infrared photometric system on the 1.5 m SRC flux collector at Tenerife on May 2 at 03.00 UT (binary phase ~0.3). The source was observed in the *J*, *H*, and *K* infrared bands, and upper limits were determined to the 99.5% confidence level for the *L* and *M* bands. Calibration of the observations was provided by monitoring the standard star SAO 62738. The resulting infrared magnitudes and fluxes for Sco X-1 in the above wave bands are given in Table 7. The values of *H* and *K* are in agreement with those found by Neugebauer *et al.*

TABLE 7

INFRARED PHOTOMETRY OF SCORPIUS X-1

	Wave Band				
	J	*H*	*K*	*L*	*M*
Flux (Jy).....	0.0269 ± .0034	0.0170 ± .0025	0.0105 ± .0016	< 0.069	< 0.87
Magnitude....	11.94 ± .15	11.99 ± .17	11.98 ± .18	> 8.86	> 5.71

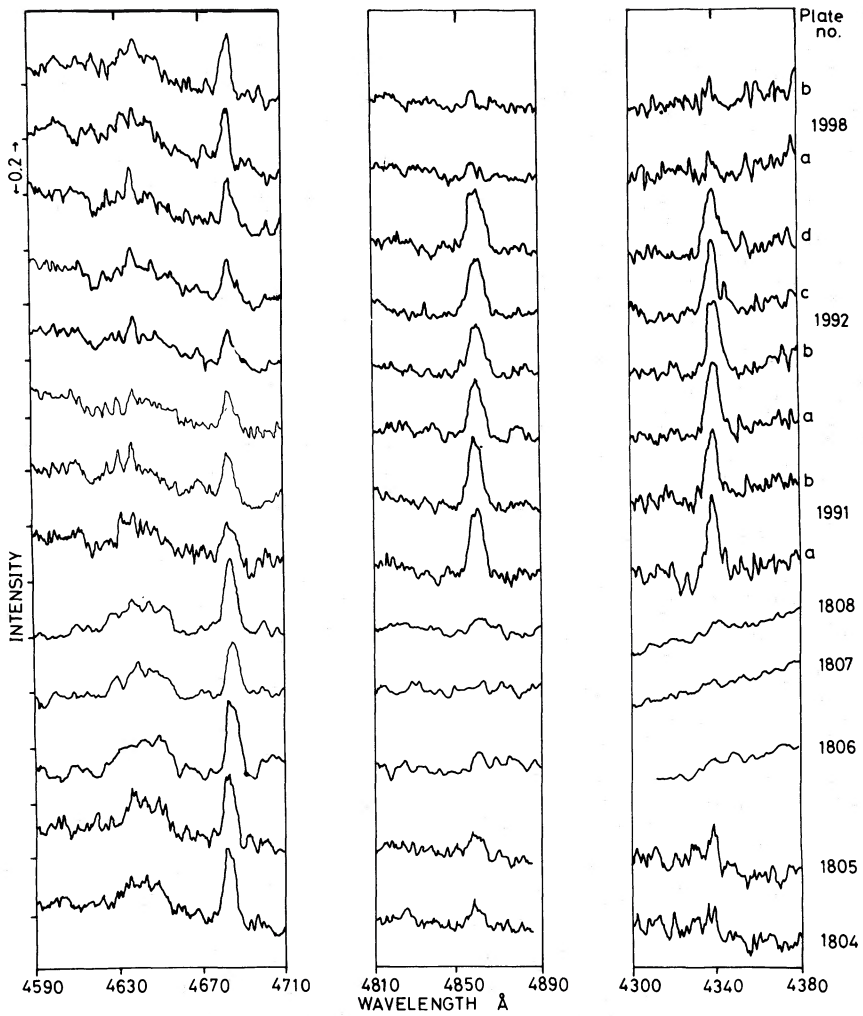

FIG. 7.—Unrectified intensity spectra of Sco X-1 obtained at SAAO, covering the region of He II λ4686, Hβ, and Hγ, respectively. The details of the plates are given in Table 5. Successive spectra have been shifted vertically by an arbitrary amount. For plates CX 1804 to CX 1807 the average spectrum is shown.

(1969). Correcting for reddening, using the color excess determined in § II*b*, gives an infrared energy distribution which, within the errors, follows a Rayleigh-Jeans law.

IV. X-RAY OBSERVATIONS OF SCORPIUS X-1

X-ray observations of Sco X-1 were recorded during the period II *IUE* observations (when the source was subsequently found to be in a low-brightness state) on July 9–10 (JD 2,443,699.33–.83). The data were obtained with the UCL–MSSL collimated proportional counter on board the *Copernicus* satellite and consist of integrated (62.5 s) photometric counts giving the intensity in the 3.8–8.8 keV range (1 count per 62.5 s = 4×10^{-11} ergs cm^{-2} s^{-1}). The reduced *Copernicus* data are shown in Figure 9, where the observed counts have been transformed to energy fluxes which are plotted against the observation time.

The source is seen to be in a quiescent state with no apparent individual X-ray bursts. The observed flux level is consistent with previous X-ray observations of Sco X-1 obtained when the source was faint; the mean value in the present data is ~4300 counts. Using the expressions given by White *et al.* (1976), the effective energy of the present *Copernicus* data is 6 keV, with the mean value of 4300 counts corresponding to a flux of 7.32×10^{-8} ergs cm^{-2} s^{-1} Å^{-1}. Unfortunately no X-ray data were recorded when the period I *IUE* observations were being obtained. However, simultaneous X-ray and *B*-magnitude monitoring of the source by White *et al.* (1976) give a *Copernicus* X-ray intensity of 7800 counts at a time when the *B*-magnitude was ~12.5. The energy range of the X-ray data of White *et al.* (1976) (2.7–8.5 keV) was slightly higher than the present observations. Nevertheless, these data strongly suggest that when the *B*-magnitude of the source changed from 12.5 to 13.3 (cf. § III*a*) the X-ray intensity underwent a similar level of change. This point will be discussed further below.

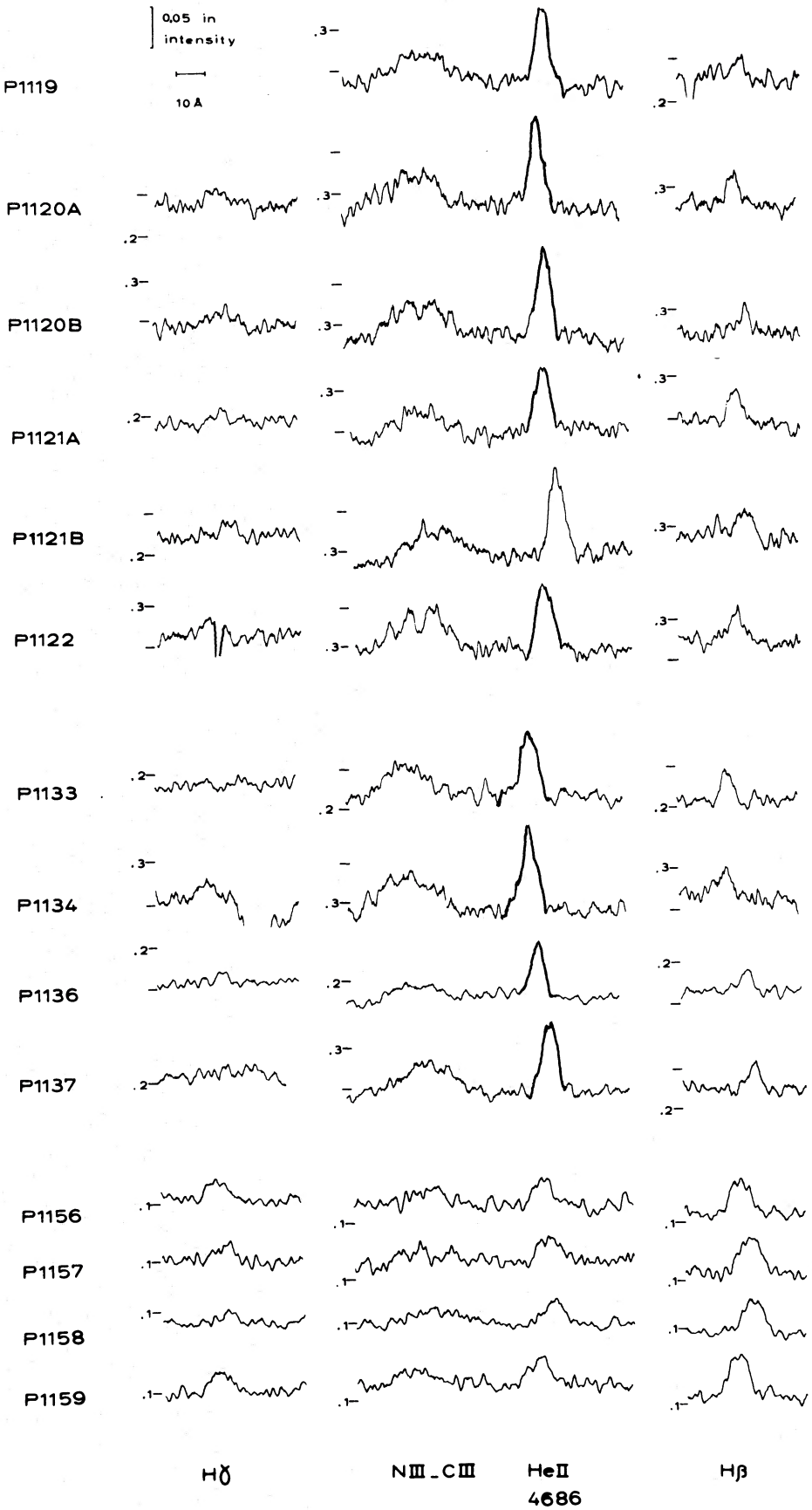

FIG. 8.—A montage of the La Silla spectra of Sco X-1 covering the features: C III/N III λ4640, He II λ4686, Hβ, and Hγ. Each spectrum is labeled by its plate number.

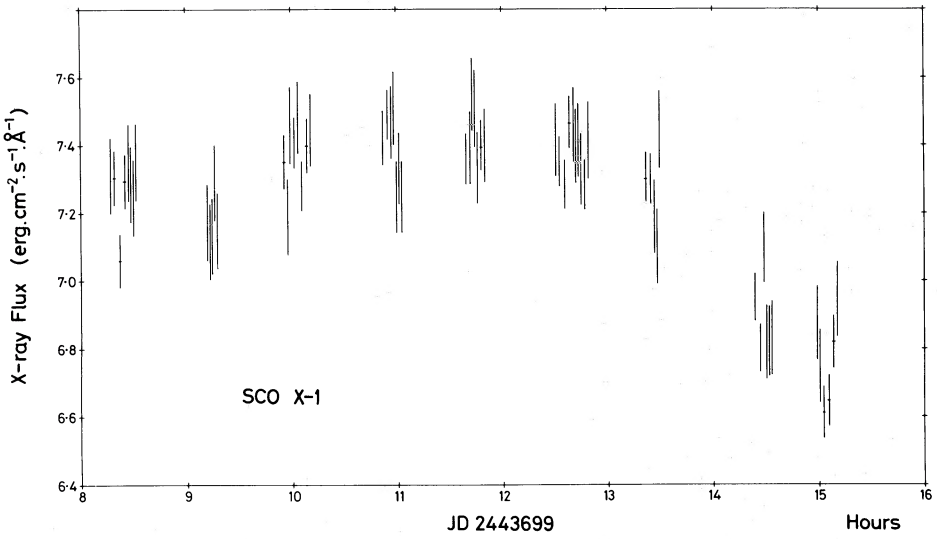

FIG. 9.—*Copernicus* X-ray observations of Sco X-1 in terms of energy fluxes (ergs cm^{-2} s^{-1} $Å^{-1}$) plotted as a function of the time of observation.

V. DISCUSSION

Two major models have been proposed to explain the observed radiation from Sco X-1 which involve the source of the visible and IR emission as either material between the component stars or the X-ray heated atmosphere of the primary star. Chodil *et al.* (1968) and Neugebauer *et al.* (1969) propose that the observed visible and IR emission, as well as the X-rays, arise from thermal bremsstrahlung emission from a hot plasma associated with the degenerate component of the system, with plasma temperatures of 4–8 $\times$ 10^7 K, depending on the level of the X-ray intensity. In both the above papers the fits to the data require the optical depth to self-absorption to be large in the visible and near-infrared. However, Mook *et al.* (1974) find that the simple bremsstrahlung model of Chodil *et al.* (1968) does not predict accurately the color-color variations observed for Sco X-1 in the Walraven photometric system, and they conclude that a more complex model is required. Milgrom (1976) has proposed that the observed visible spectrum (and ultraviolet) is the result of heating of the surface of the primary star (nondegenerate component) by the X-ray emission from the secondary, with spectral and brightness changes resulting from both variable X-ray emission and binary-phase–related changes in the heating of the primary atmosphere and its orientation with respect to the observer's line of sight.

During the period II observations described herein, Sco X-1 underwent a substantial decrease in its ultraviolet and visible emission over the corresponding values found in period I. Clearly a good test of the two models outlined above for the source is a comparison of these bright and faint state data. The changes that occur between these two states, described previously, are summarized as follows:

i) The first is an inferred X-ray intensity decrease by a factor of $\sim$2.

ii) The *B*-magnitude changes from $\sim$12.5 to 13.3.

iii) The UV brightness level over the wavelength range 1150–3200 Å changes by a factor of $\sim$2.

iv) Significant changes in the strengths of the UV and visible emission lines occur, with those arising in the highest ionization species changing most.

v) No significant change occurs in the shape of the UV energy distribution or in the colors ($U_\lambda - B$).

This latter point is illustrated in Figure 10, where the difference in magnitudes in the UV data (Fig. 3) is plotted against those in the B band (Fig. 6) for those observations which were recorded simultaneously. The full line in Figure 10 is the expected correlation for no color changes. It is clear from these data that the color

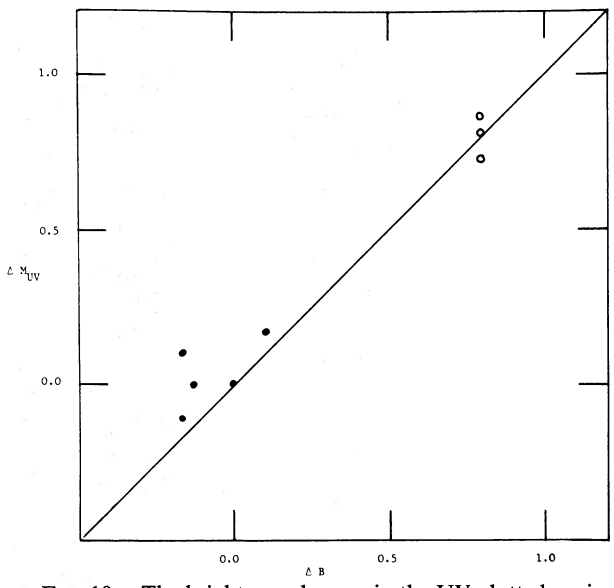

FIG. 10.—The brightness changes in the UV plotted against those in the visible B band for simultaneous *IUE* and visible observations. The UV data are relative to SWP 1470 and LWR 1434, and the visible data are relative to the *B*-magnitudes at the time of the above two *IUE* observations.

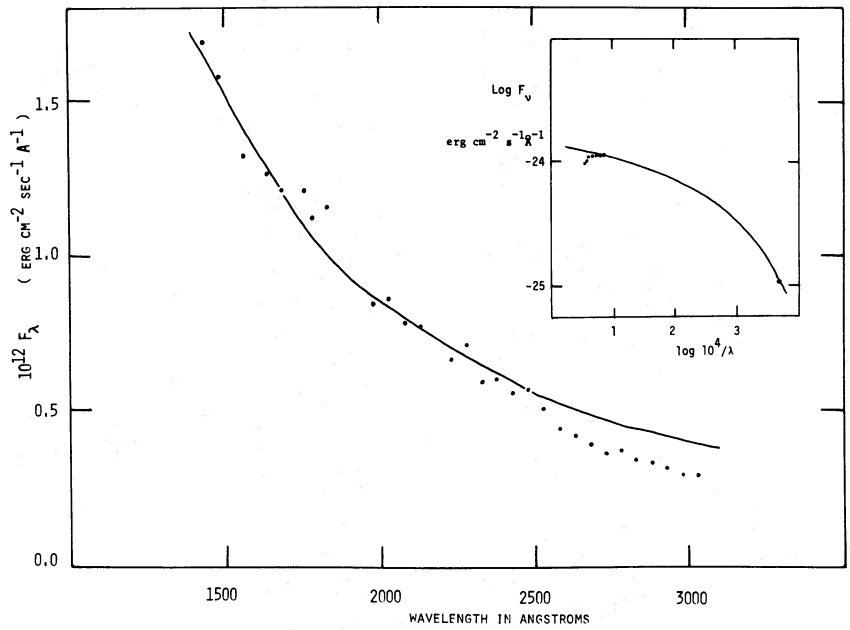

FIG. 11.—The UV continuum energy distribution of Sco X-1 obtained from images SWP 1953 and LWR 1804, corrected for interstellar reddening with $E_{B-V} = 0.35$, compared to the thermal bremsstrahlung model at $kT = 7$ keV of Chondil *et al.* (1968). The model distribution has been normalized to the observed X-ray flux at 6 keV measured simultaneously with the above two *IUE* observations. *Insert:* the combined X-ray and UV data discussed above plotted together and compared with the thermal bremsstrahlung model.

changes are small (<0.1 mag.), although the actual brightness of the source in the visible and UV has changed by ~0.8 mag. Mook (1970) has reported $(B - V)$ color changes in Sco X-1 which are well correlated with changing V from 12.2–13.2 mag, with the source becoming redder at fainter brightness levels. However, the amplitude of these $(B - V)$ variations (≤ 0.1 mag) is close to that which would be detectable in our $(U_\lambda - B)$ colors, the accuracy of which is governed by the photometric errors in the *IUE* data. Thus, although we cannot detect small color variations of the kind reported in the visible, the present observations indicate no substantial increase in color variation in the ultraviolet.

It seems difficult to reconcile the observed $(U_\lambda - B)$ color constancy with the model for the source proposed by Milgrom (1976), where the visible and UV emission arises from the X-ray heated surface of the primary star. Substantial changes would surely be expected to occur in such a heating effect, if the incident X-ray intensity changes by a factor of 2, with associated changes in the level and color temperature of the emitted UV and visible radiation. However, qualitatively the thermal bremsstrahlung model could predict an approximate color constancy over the UV–visible wavelength range with changing X-ray emission. For an optically thin plasma the thermal bremsstrahlung flux $F_\lambda \propto \lambda^{-2} \exp(-hc/\lambda kT)$. For high values of kT, say 5–20 keV, the exponential term remains approximately constant for wavelengths in the UV and visible, and thus over this wavelength range the broad shape of the flux distribution would be independent of kT, or X-ray intensity, as observed. The effect of electron scattering, particularly important at X-ray wavelengths (Lamb and Sanford 1980), may not significantly alter this picture in the UV and visible. Further support for the bremsstrahlung model is given by the simultaneous *IUE* (SWP 1953, LWR 1804) spectra and *Copernicus* X-ray observations (§ IV). The observed X-ray flux of 7.32×10^{-8} ergs cm^{-2} s^{-1} Å^{-1} is very close to that observed by Chodil *et al.* (1968), also when the source was in an optically faint state. Chodil *et al.* (1968) find a good fit to their low-intensity X-ray data over the energy range of 2–20 keV with a thermal bremsstrahlung model with $kT = 7$ keV. The present simultaneous X-ray and UV data are shown in Figure 11, together with this latter bremsstrahlung model normalized at the effective *Copernicus* energy of 6 keV. The model distribution fits the observed UV distribution extremely well, particularly in the range λλ1300–2000. The small differences at longer wavelengths can easily be explained in terms of increasing self-absorption optical-depth effects with increasing wavelength as expected.

Chodil *et al.* (1968) find a best fit to their observed high-intensity X-ray data with a bremsstrahlung model at $kT = 4$ keV. This gives a distribution of $F_\lambda \propto \lambda^{-2.3}$ in the *IUE* wavelength range. The de-reddened UV energy distribution for the high-brightness state data of Sco X-1 shown in Figure 4 result in an observed $F_\lambda \propto \lambda^{-2.4}$ for $E_{B-V} = 0.35$, in close agreement with the Chodil *et al.* (1968) model. The absolute SWP fluxes observed are also close (within 20%) to those predicted in the bremsstrahlung model. The heated atmosphere model (Milgrom 1976) predicts a much flatter spectrum shortward of 3000 Å. The present

observations therefore appear to favor the thermal bremsstrahlung model for the system.

The emission-line spectrum clearly must arise in a different region from the high-temperature plasma ($kT \geq 4$ keV), since the level of ionization inferred from the observed UV and visible lines is considerably lower than would otherwise be expected. The present observations do not rule out either a more extensive, lower temperature, emission-line region surrounding the higher temperature continuum plasma or the heated surface of the primary star. The observed changes in the strengths of the UV and visible emission lines are consistent in either case with expected changes in ionization conditions caused by a variable X-ray flux. Detailed modeling of these lines in the two cases will probably be needed to fix the location of their source, as well as the physical and chemical conditions in that region.

We would like to thank the *IUE* Project personnel at the GSFC and Madrid Ground Stations for their assistance in obtaining the *IUE* observations. We thank Dr. M. J. Selby for the use of his near-infrared photometric system at Tenerife and the staff of the European Southern Observatory, La Silla, Chile. M. Burger acknowledges the support of an ESA Fellowship. We thank an anonymous referee for some useful comments and for bringing to our attention some important references. Dr. Paul Lamb provided helpful comments on the bremsstrahlung model fits.

REFERENCES

Boggess, A., *et al.* 1978*a*, *Nature*, **275**, 372.
Boggess, A., *et al.* 1978*b*, *Nature*, **275**, 377.
Bohlin, R. C., Carnochan, D. J., Holm, A., Savage, B. D., and Snijders, M. A. J. 1978, *IUE* Project Memorandum.
Chodil, G., *et al.* 1968, *Ap. J.*, **154**, 645.
Cowley, A., and Crampton, D. 1975, *Ap. J.* (*Letters*), **201**, L65.
Crampton, D., Cowley, A., Hutchings, J. B., and Kaat, C. 1976, *Ap. J.*, **207**, 907.
Giacconi, R., Gursky, H., Paolini, F., and Rossi, B. 1962, *Phys. Rev. Letters*, **9**, 439.
Gottlieb, E. W., Wright, E. L., and Liller, W. 1975, *Ap. J.* (*Letters*), **195**, L33.
Hiltner, W. A., and Mook, D. E. 1970, *Ann. Rev. Astr. Ap.*, **8**, 139.
Ilovaisky, S. A. 1978, private communication.
Lamb, P., and Sanford, P. W. 1980, *M.N.R.A.S.*, **188**, 555.
Milgrom, M. 1976, *Ap. J.*, **208**, 191.
Miyamoto, S., and Matsuoka, M. 1977, *Space Sci. Rev.*, **20**, 687.
Mook, D. 1970, *Ap. J.*, **161**, 1165.
Mook, D., Hiltner, W. A., and Lynds, R. 1971, *Ap. J.* (*Letters*), **163**, L69.
Mook, D., Edwards, S., and Hiltner, W. A. 1972, *Ap. J.* (*Letters*), **177**, L63.
Mook, D., Messina, R. J., Pel, J., and Hiltner, W. A. 1974, *Ap. J.*, **191**, 493.
Mook, D., *et al.* 1975, *Ap. J.*, **197**, 425.
Nandy, K., Thompson, G. I., Jamar, C., Monfils, A., and Wilson, R. 1975, *Astr. Ap.*, **44**, 195.
Nandy, G. I., Thomson, G. I., Jamar, C., Monfils, A., and Wilson, R. 1976, *Astr. Ap.*, **51**, 63.
Neugebauer, G., Oke, J. B., Beklin, E., and Garmire, G. 1969, *Ap. J.*, **155**, 1.
Sandage, A. R., *et al.* 1966, *Ap. J.*, **146**, 316.
Wu, C-C. 1979, *Ap. J.*, **227**, 291.
White, N. E., Mason, K. O., Sanford, P. W., Ilovaisky, S. A., and Chevalier, C. 1976, *M.N.R.A.S.*, **176**, 91.

J. Black, R. J. Davis, A. K. Dupree, H. Gursky, L. Hartmann, and J. Raymond: Center for Astrophysics, 60 Garden Street, Cambridge, MA 02138

M. Burger: Astronomical Institute, Space Research Laboratory, Beneluxlaan 21, Utrecht, The Netherlands

C. de Loore: Astrophysics Institute, Vrije Universiteit Brussel, Pheinlaan 2, 8-1050, Brussels, Belgium

R. D. Joseph and W. P. S. Meikle: Blackett Laboratory, Imperial College of Science and Technology, Prince Consort Road, London SW7, England

T. Matilsky: Physics Department, Rutgers University, Piscataway, NJ 08854

J. Menzies and P. Whitelock: South African Astronomical Observatory, P.O. Box 9, Observatory, Cape Province, South Africa

G. Pollard and P. Sanford: Mullard Space Science Laboratory, Holmbury St. Mary, Dorking, Surrey, England

M. C. W. Sandford: SRC Appleton Laboratory, Ditton Park, Slough SL3 9JX, Berks, England

F. Sanner and P. Vanden Bout: Department of Astronomy, University of Texas, Austin, TX 78712

E. L. van Dessel: Royal Belgium Observatory, Ringlaan 3, B-1180, Brussels, Belgium

A. J. Willis and R. Wilson: Department of Physics and Astronomy, University College London, Gower Street, London WC1E 6BT, England